Computational and Structural Biotechnology Journal 21 (2023) 2884–2898

Contents lists available at ScienceDirect

Computational and Structural Biotechnology Journal

journal homepage: www.elsevier.com/locate/csbj

Research Article

Structural characterization of the *Aspergillus niger* citrate transporter CexA uncovers the role of key residues S75, R192 and Q196

J. Alves [a,b,1], M. Sousa-Silva [a,b,1], P. Soares [a,b], M. Sauer [c,d], M. Casal [a,b], I. Soares-Silva [a,b,*]

[a] Centre of Molecular and Environmental Biology (CBMA), Department of Biology, University of Minho, Campus de Gualtar, 4710-057 Braga, Portugal
[b] Institute of Science and Innovation for Bio-Sustainability (IB-S), University of Minho, Campus de Gualtar, 4710-057 Braga, Portugal
[c] University of Natural Resources and Life Sciences, Vienna, Department of Biotechnology, Institute of Microbiology and Microbial Biotechnology, Muthgasse 18, 1190 Vienna, Austria
[d] Austrian Centre of Industrial Biotechnology (ACIB GmbH), Muthgasse 11, 1190 Vienna, Austria

ARTICLE INFO

Article history:
Received 9 January 2023
Received in revised form 25 April 2023
Accepted 25 April 2023
Available online 26 April 2023

Keywords:
Carboxylic acids
Import
Export
Site-directed mutagenesis
Heterologous expression in yeast

ABSTRACT

The *Aspergillus niger* CexA transporter belongs to the DHA1 (Drug-H$^+$ antiporter) family. CexA homologs are exclusively found in eukaryotic genomes, and CexA is the sole citrate exporter to have been functionally characterized in this family so far. In the present work, we expressed CexA in *Saccharomyces cerevisiae*, demonstrating its ability to bind isocitric acid, and import citrate at pH 5.5 with low affinity. Citrate uptake was independent of the proton motive force and compatible with a facilitated diffusion mechanism. To unravel the structural features of this transporter, we then targeted 21 CexA residues for site-directed mutagenesis. Residues were identified by a combination of amino acid residue conservation among the DHA1 family, 3D structure prediction, and substrate molecular docking analysis. *S. cerevisiae* cells expressing this library of CexA mutant alleles were evaluated for their capacity to grow on carboxylic acid-containing media and transport of radiolabeled citrate. We also determined protein subcellular localization by GFP tagging, with seven amino acid substitutions affecting CexA protein expression at the plasma membrane. The substitutions P200A, Y307A, S315A, and R461A displayed loss-of-function phenotypes. The majority of the substitutions affected citrate binding and translocation. The S75 residue had no impact on citrate export but affected its import, as the substitution for alanine increased the affinity of the transporter for citrate. Conversely, expression of CexA mutant alleles in the *Yarrowia lipolytica cex*1Δ strain revealed the involvement of R192 and Q196 residues in citrate export. Globally, we uncovered a set of relevant amino acid residues involved in CexA expression, export capacity and import affinity.

1. Introduction

Carboxylic acids are weak organic acids displaying great applicability in the food, pharmaceutical, cosmetic, and polymer sectors [1]. Citric acid is one of the most relevant chemicals in the world produced via microbial fermentation, and is utilized as a preservative, acidulant, emulsifier, flavouring, sequestrant, and buffering agent [2]. With a global market of 2.4 million tons in 2020, citric acid demand is still increasing and is expected to reach 2.9 million tons in 2026 [3]. Several microorganisms are able to produce citric acid, including filamentous fungi, yeast, and bacteria [2,4]. The industrial production of citric acid by *Aspergillus niger* dates back to 1923, and it is still the major method for microbial production of citric acid in large-scale fermentations [4]. The capacity of *A. niger* to secrete organic acids and proteins to the extracellular media, combined with its tolerance to extreme acid environments, contributes to its relevance as an industrial microbial cell factory [5].

In an age that works towards a circular bioeconomy, several microorganisms have been metabolically engineered to use specific substrates such as industrial wastes and sub-products, to produce high-value metabolites [1]. The transport of such compounds across cell membranes and cellular metabolism are key steps in the optimization of microbial cell factories. This need has leveraged the engineering of plasma membrane transporters towards the

* Corresponding author at: Centre of Molecular and Environmental Biology (CBMA), Department of Biology, University of Minho, Campus de Gualtar, 4710-057 Braga, Portugal.
E-mail address: ijoao@bio.uminho.pt (I. Soares-Silva).
[1] Shared authorship

https://doi.org/10.1016/j.csbj.2023.04.025

improved assimilation of substrates and the export of metabolites of interest [6,7]. Engineering strategies comprise the expression of specific importer and/or exporter proteins with improved properties regarding transport stability, capacity and specificity [1,7,8]. Despite the existence of a significant number of carboxylate importers functionally characterized in fungi, few exporters have been identified to this day [1]. Itp1 and MfsA are itaconate exporters from *Ustilago maydis* [9] and *Aspergillus terreus* [10], respectively, and members of the Major Facilitator Superfamily, although not reciprocal best hits in terms of sequence identity [11]. Mae1p, a member of the Tellurite-resistance/Dicarboxylate Transporter Family from *Schizosaccharomyces pombe,* exports fumarate, succinate, and malate [12,13]. In *S. cerevisiae*, Jen1 (Sialate:H^+ Symporter family) and Ady2 (Acetate Uptake Transporter family) are able to mediate the export of lactic acid [14].

Recent studies have reported two citrate exporters: CexA from *A. niger* [6,15] a member of the Drug-H^+ Antiporter family, and Cex1 from *Yarrowia lipolytica* [16] a member of the Drug:H^+ Antiporter 2 family. The production of citric acid was impaired in *A. niger* upon the disruption of CexA, while its heterologous expression in *S. cerevisiae* promoted the secretion of citric acid when cells were grown on glucose [6,15]. CexA is the main plasma membrane transporter for citric acid in *A. niger.* Its overexpression led to significant increases in secreted citric acid, demonstrating how the manipulation of a single plasma membrane exporter can significantly improve citric acid secretion [6]. Furthermore, the engineering of CexA homologs from *Aspergillus luchuensis* mut. *kawachii*, (*Ak*CexA) and *Aspergillus oryzae* (*Ao*CexA and *Ao*CexB) demonstrated that the expression level of these transporters is a key factor for citric acid productivity in these strains [17]. Distinct molecular mechanisms were suggested for citrate export in *A. niger* - passive diffusion, citrate/H^+ antiporter, and a ΔpH-driven symport with H^+ [18] – but the de facto energetics of the transporter remains unclear. In the present study, we characterized the kinetics, energetics, and specificity of CexA expressed in *S. cerevisiae*. By using a rational site-directed mutagenesis approach, we identified amino acid residues essential for CexA activity and, in particular, key residues crucial for the export of citrate. Finally, selected mutant alleles were expressed in *Y. lipolytica* disrupted in its native citrate exporter (Cex1). Cultivation in bioreactors allowed us to determine the role of these residues in citrate export.

2. Materials and methods

2.1. Strains, plasmids, and growth conditions

The plasmids, yeast strains and oligonucleotides utilized in this work are described in Tables 1, 2, and S1, respectively. The strains *Saccharomyces cerevisiae* CEN.PK 113-5D [19] and *Yarrowia lipolytica* DSM 3286 [16] were used as hosts for the heterologous expression of CexA. The multicopy plasmids constructed by Steiger et al. [6] were used for the expression of CexA in *S. cerevisiae* under the control of the constitutive *S. cerevisiae* promoters *TPI1* or *TEF1*. The *S. cerevisiae* CEN.PK 113-5D transformants were maintained on YP glucose 2 % (w/v) supplemented with 0.3 mg/mL hygromycin B [6]. Yeast cells were grown in Difco yeast nitrogen base (BD Life Sciences, MD, USA), 0.67% w/v (YNB medium), supplemented with adequate requirements for prototrophic growth. Carbon sources utilized: glucose (2.0 % w/v), lactic acid (0.5 % v/v, pH 5.0), acetic acid (0.5 % v/v, pH 6.0), pyruvic acid (0.5 % w/v, pH 5.0), succinic acid (1.0 % w/v, pH 5.0), fumaric acid (1.0 % w/v, pH 5.0), malic acid (1.0 % w/v, pH 5.0) and citric acid (1.0 % w/v, pH 5.5). The culture media pH was adjusted with NaOH solution (12 M). For the evaluation of *S. cerevisiae* growth phenotypes by spot assays, cells were grown on YNB glucose without uracil (YNB Glu−Ura) media, until the mid-exponential phase. Initially, the optical density at 640 nm (OD_{640}) was adjusted to 0.1 and a set of three 1:10 serial dilutions were performed; 3.0 μL of each suspension were inoculated into the desired media, using YNB Glu−Ura as a control carbon source. Cells were incubated at 30 °C for 4 days. Cell growth of *S. cerevisiae* was also evaluated in YNB liquid media containing acetic acid (0.5 % v/v, pH 6.0) or glucose (2.0 % w/v), at 30 °C, both in duplicates. The supernatants were collected for the quantification of citrate, acetate and glucose concentration by HPLC analysis with an Auto Sampler L-2200 Elite LaChrom chromatograph coupled to a Refractive Index (RI) L-2490 detector (Hitachi, Berkshire, United Kingdom) and a Rezex ROA-Organic Acid H^+ (8 %) Ion Exclusion column (Phenomenex, CA, USA). The column was operated at 40 °C with 2.5 mM H_2SO_4 as the mobile phase and a flow rate of 0.5 mL/min for 25 min.

Table 1
List of plasmids utilized in this work.

Plasmid	Characteristics	Reference
pϕ	BB3_arscen_URA_Hygro	[6]
pCexA-1; pCexA	pMST-1313; cassette p*TEF1-cexA*-t*CYC1*	[6]
pCexA-2	pMST-1312; cassette p*TPI1-cexA*-t*CYC1*	[6]
pJen1::GFP	p416GPD derivative, constitutive expression of JEN1::GFP	[21]
pCexA::GFP	pMST-1313 derivative, constitutive expression of CexA::GFP	This work
pϕ-Yl	pMEG_BB3_YL68N_AB used for negative control in *Y. lipolytica* cultivations	[22]
pYl-CexA	pMEG_BB3_YL68N_AB; cassette p*TEF1-cexA*-t*CYC1*	This work

2.2. Transport assays

Measurement of transport activity was performed as previously described [20] using [1,5-^{14}C] citric acid (Perkin Elmer, MA, USA) with a specific activity of 300 and 1500 dpm/nmol. Cells were harvested by centrifugation, washed twice in ice-cold deionized water and resuspended in ice-cold deionized water to a final concentration between 25 and 35 mg cell dry weight/mL. The reaction mixtures were prepared in microtubes containing 60 μL of 0.1 M KH_2PO_4 at the desired pH and 30 μL of the yeast cell suspension. After 2 min of incubation at 30 °C, the reaction was started by the addition of 10 μL of a solution of the radiolabelled substrate at the desired pH and concentration. After 15–30 s, the reaction was stopped by the addition of 100 μL of a cold non-labelled substrate (100-fold concentrated). The suspension was centrifuged for 7 min at 13,200 rpm. The supernatant was carefully rejected, and the pellet was resuspended in 1 mL of deionized cold water and centrifuged for 10 min at 13,200 rpm. The pellet was resuspended in 1 mL of the scintillation liquid Opti-Phase HiSafe 3 (Perkin Elmer, MA, USA). Radioactivity was measured in a Tri-Carb 4810TR liquid scintillation spectrophotometer (Perkin Elmer, MA, USA), with disintegrations per minute correction. The GraphPad Prism (San Diego, CA, USA) v4.0 for Windows was used to estimate the kinetic parameters using a non-linear regression analysis, and the unpaired t-test was used to determine the statistical significance $P < 0.05$. The data shown correspond to the mean values of at least three independent experiments, with three replicas of each one. The inhibition effect of non-labelled substrates on the initial uptake velocities of labelled citric acid was assayed by adding simultaneously the labelled and non-labelled substrates. Non-specific ^{14}C adsorption to the cells, as well as the diffusion component, was determined with a mixture of unlabelled acid 1000-fold concentrated and labelled acid, according to the methodology previously established [21].

2.3. Phylogenetic reconstruction of CexA

A total of around 10,000 proteomes were retrieved from the refseq subsection of the NCBI Assembly platform. The individual FASTA

Table 2
Yeast strains utilized in this work.

Strain	Genotype	Reference
S. cerevisiae CEN.PK113–5D	*MAT*a *MAL2–8C SUC2 ura3–52*	[19]
S. cerevisiae CEN.PK 113–5D pϕ	*S. cerevisiae* CEN.PK113–5D transformed with arscen plasmid, empty vector	[6]
S. cerevisiae pCexA (1); cE(p*TEF1*)-CexA	*S. cerevisiae* CEN.PK113–5D transformed with p*TEF1-cexA*-t*CYC1* cassette	[6]
S. cerevisiae pCexA (2); cE(p*TPI1*)-CexA	*S. cerevisiae* CEN.PK113–5D transformed with p*TPI1-cexA*-t*CYC1* cassette	[6]
S. cerevisiae pCexA-S71A	*S. cerevisiae* CEN.PK 113–5D transformed with pCexA-S71A	This work
S. cerevisiae pCexA-S75A	*S. cerevisiae* CEN.PK 113–5D transformed with pCexA-S75A	This work
S. cerevisiae pCexA-N76A	*S. cerevisiae* CEN.PK 113–5D transformed with pCexA-N76A	This work
S. cerevisiae pCexA-P80A	*S. cerevisiae* CEN.PK 113–5D transformed with pCexA-P80A	This work
S. cerevisiae pCexA-D84A	*S. cerevisiae* CEN.PK 113–5D transformed with pCexA-D84A	This work
S. cerevisiae pCexA-G122A	*S. cerevisiae* CEN.PK 113–5D transformed with pCexA-G122A	This work
S. cerevisiae pCexA-R123A	*S. cerevisiae* CEN.PK 113–5D transformed with pCexA-R123A	This work
S. cerevisiae pCexA-R124A	*S. cerevisiae* CEN.PK 113–5D transformed with pCexA-R124A	This work
S. cerevisiae pCexA-R154A	*S. cerevisiae* CEN.PK 113–5D transformed with pCexA-R154A	This work
S. cerevisiae pCexA-F188A	*S. cerevisiae* CEN.PK 113–5D transformed with pCexA-F188A	This work
S. cerevisiae pCexA-R192A	*S. cerevisiae* CEN.PK 113–5D transformed with pCexA-R192A	This work
S. cerevisiae pCexA-Q196A	*S. cerevisiae* CEN.PK 113–5D transformed with pCexA-Q196A	This work
S. cerevisiae pCexA-P200A	*S. cerevisiae* CEN.PK 113–5D transformed with pCexA-P200A	This work
S. cerevisiae pCexA-T207A	*S. cerevisiae* CEN.PK 113–5D transformed with pCexA-T207A	This work
S. cerevisiae pCexA-P235A	*S. cerevisiae* CEN.PK 113–5D transformed with pCexA-P235A	This work
S. cerevisiae pCexA-E236A	*S. cerevisiae* CEN.PK 113–5D transformed with pCexA-E236A	This work
S. cerevisiae pCexA-T237A	*S. cerevisiae* CEN.PK 113–5D transformed with pCexA-T237A	This work
S. cerevisiae pCexA-Y307A	*S. cerevisiae* CEN.PK 113–5D transformed with pCexA-Y307A	This work
S. cerevisiae pCexA-S311A	*S. cerevisiae* CEN.PK 113–5D transformed with pCexA-S311A	This work
S. cerevisiae pCexA-S315A	*S. cerevisiae* CEN.PK 113–5D transformed with pCexA-S315A	This work
S. cerevisiae pCexA-R461A	*S. cerevisiae* CEN.PK 113–5D transformed with pCexA-R461A	This work
S. cerevisiae pCexA::GFP	*S. cerevisiae* CEN.PK 113–5D transformed with pCexA::GFP	This work
Y. lipolytica DSM 3286 *Cex1*Δ	*Y. lipolytica* DSM 3286 with Cex1 citrate exporter deleted	[16]
Y. lipolytica pϕ	*Y. lipolytica* DSM 3286 *Cex1*Δ transformed with pϕ-Yl	This work
Y. lipolytica pCexA	*Y. lipolytica* DSM 3286 *Cex1*Δ transformed with pYl-CexA	This work
Y. lipolytica pCexA-S75A	*Y. lipolytica* DSM 3286 *Cex1*Δ transformed with pYl-CexA-S75A	This work
Y. lipolytica pCexA-P80A	*Y. lipolytica* DSM 3286 *Cex1*Δ transformed with pYl-CexA-P80A	This work
Y. lipolytica pCexA-R192A	*Y. lipolytica* DSM 3286 *Cex1*Δ transformed with pYl-CexA-R192A	This work
Y. lipolytica pCexA-Q196A	*Y. lipolytica* DSM 3286 *Cex1*Δ transformed with pYl-CexA-Q196A	This work

files were converted into a local database. To avoid redundancies, only sequences derived from a single genome from a particular species were selected for the database [23] considering the genome of that species with the highest number of proteins described. A BLAST search using the protein XP_025452994.1 from *Aspergillus niger* as a query was done in the local database; the data obtained was filtered with a cut-off e-value of 10^{-10} and an associated query-cover value higher than 65 %. Protein sequences were aligned with the online server MAFFT [24]. Sequences not aligning extensively throughout the conserved region were removed from the subsequent phylogenetic analysis. These low-quality alignments could result from the lower quality of the stretch of the genome where the sequences are located as well as from an incomplete gene annotation and they could still be functional genes, although unusable in the phylogenetic reconstruction. A Maximum Likelihood algorithm was used for the phylogenetic reconstruction using MEGA7 [25] under the Jones-Taylor-Thornton substitution model using a Bootstrap of 1000 repetitions [26]. The FigTree v.1.4.4. software (http://tree.bio.ed.ac.uk/) was used for phylogenetic tree visualization and edition.

2.4. CexA site-directed mutagenesis and functional analysis in Saccharomyces cerevisiae

Site-directed mutagenesis was performed on the pTEF1-CexA plasmid, as previously described [21], resulting in 21 mutant CexA alleles (Table 1). The mutagenesis was performed with Accuzyme DNA Polymerase (Meridian Bioscience, TN, USA) using the pCexA-1 as a template (20 ng) and the complimentary oligonucleotides containing the desired substitution described in Table S1. PCR reaction: 30 s at 95º C, 18 cycles of 30 s at 95º C, 60 s at the oligonucleotide Tm, 8 min at 68º C, and a final extension step of 10 min at 68º C. To destroy the parental strands, the PCR reaction was incubated with the restriction enzyme *Dpn*I (NZYTEC, Lisbon, Portugal) for 2 h at 37º C. This mixture was then used to transform *E. coli* and plasmid extraction was performed with the NZYMiniprep (NZYTEC, Lisbon, Portugal). The sequences of CexA mutant alleles were confirmed by sequencing (Eurofins Genomics, Ebersberg, Germany). CexA alleles were expressed in *S. cerevisiae* CEN.PK 113–5D (Table 2) strain [27] and transformants were selected by the complementation of uracil auxotrophy.

The insertion of the GFP tag in the C-terminal of CexA was done using the gap-repair technique [28]. Briefly, the linearization of the plasmid was done through PCR reaction using the Linear_F and the Pseq_R primers with 20 cycles: 30 s at 95 °C; 1 min at 68.8 °C; and 8 min at 72 °C. The amplification of the GFP was done via PCR in 30 cycles using the GFP GR_F and GFP GR_R primers: 30 s at 95 °C; 30 s at 75 °C; and 90 s at 72 °C. In a stoichiometric ratio of 2:1 (insert:vector) the mix of the DNA was transformed into *Escherichia coli* XL1-blue using the heat shock transformation protocol. The transformants presenting resistance to Hygromycin B were selected for further evaluation. The constructions were confirmed by sequencing and transformed in the *S. cerevisiae* CEN.PK 113–5D strain [27]. Transformants were selected by complementation of the uracil auxotrophy. For the evaluation of protein localization, cells were grown overnight in YNB Glu–Ura, collected during the exponential growth phase, and visualized with the fluorescence microscope BX63, coupled with a digital camera DP74 and the image analysis software cellSens Dimension v.2.3 (Olympus, Hamburg, Germany).

2.5. CexA structure prediction and molecular docking

The CexA transmembrane segments (TMSs) were predicted with the TMHMM software (http://www.cbs.dtu.dk/services/TMHMM-2.0/). The predicted 3D structure of CexA (XP_001398400.1) was obtained using the HHpred [29] and AlphaFold [30]. For the HHpred

prediction, the L-lactate transporter from *Syntrophobacter fumaroxidans* (PDB 6G9X; 2.54 Å resolution) was used as a template [31]. The Alphafold AF-G3Y4N5-F1-model_v4 structure was used in this work. The molecular docking simulations of citrate binding to CexA were done as previously described [20]. Deprotonated forms of citric acid, having the protonation states adjusted to match the desired pH, were used for substrate docking simulations. The substrates' 3D structures were built by inputting canonical SMILES strings in the UCSF Chimera [32], being minimized before molecular docking simulations in PyRx software [33] with AutoDock Vina. Chimera and Maestro v11.2 were used for visualizing the predicted interactions and 3D structures. The pore radius was predicted as previously described [34] using the HOLE (2.2.005 Linux) [35] and the Visual Molecular Dynamics (VMD) v1.9.3 software [36]. The pore radius was visualized on a graph with the X-axis presenting the coordinates along the protein pore.

2.6. CexA expression in Yarrowia lipolytica and bioreactor cultivation

The mutant alleles S75A, P80A, R192A and Q196A were expressed in the *Y. lipolytica* DSM 3286 strain with the native citrate exporter (Cex1) deleted. The plasmids containing the *CEXA* mutant alleles were constructed using the Golden Gate Cloning (GGC) method in *Escherichia coli* DH10B using the *TEF1* and *CYC1* as promoter and terminator, respectively, as previously described [22]. The batch fermentations in bioreactors were done in triplicate, in a DASGIP Parallel Bioreactor System (Eppendorf Hamburg, Germany) with four parallel bioreactors and a maximum working volume of 1.2 L [37]. The preculture was grown on YPD media with 400 mg/L nourseothricin at 30 °C and 180 rpm and used to inoculate 500 mL of media to a final OD_{640} of 1. The media used for the fermentation had the following composition per litre: 100 g glycerol, 3.1 g $(NH_4)_2SO_4$, 1.0 g KH_2PO_4, 1.3 g $Na_2HPO_4 \cdot 2\ H_2O$, 1.0 g $MgSO_4 \cdot 7\ H_2O$, 0.2 g $CaCl_2 \cdot 2\ H_2O$, 0.5 g citric acid, 21 mg $FeCl_3$, 1 mg Thiamine-HCl, 0.5 mg H_3BO_3, 0.06 mg $CuSO_4 \cdot 5\ H_2O$, 0.1 mg KI, 0.45 mg $MnSO_4 \cdot H_2O$, 0.71 mg $ZnSO_4 \cdot 7\ H_2O$, 0.23 mg $Na_2MoO_4 \cdot 2\ H_2O$ and 400 mg nourseothricin. Due to the production of foam, 5 % (w/v) Struktol (SB 2121; Schiller+Seilacher GmbH) was added to the bioreactor when needed. Dissolved oxygen and pH were monitored (VisiFerm DO 120 and Mettler-Toledo probe, respectively) and maintained at 50 % and pH 5.5, respectively. Glycerol, citrate, erythritol, arabitol, mannitol and α-ketoglutarate concentration were determined by HPLC analysis with an Aminex HPX-87 H column 300 × 7.8 mm (Bio-Rad Laboratories, CA, USA) as previously described [37]. The yeast cultures were also monitored considering OD and cell dry mass, both in duplicates. For cell dry mass determination 2 mL of culture were collected and centrifuged at 10,000 g for 5 min. The pellet was washed with deionized water and dried for 2 days at 100 °C. An unpaired *t*-test, at a significance level $p < 0.05$, was done in GraphPad Prism (San Diego, CA, USA) v4.0 for Windows to probe for statistical differences among the data collected for the distinct strains.

3. Results

3.1. Functional studies of CexA in Saccharomyces cerevisiae CEN.PK 113–5D

Expression of CexA in *Saccharomyces cerevisiae* was performed under the control of the constitutive promoters *TEF1* or *TPI1* (Fig. 1 A). The expression of CexA under the control of the *TEF1* promoter resulted in a more evident impaired growth on carboxylic acids than the *TPI1* promoter, when compared with the growth phenotype of cells transformed with the empty plasmid. Thus, the expression vector containing the *TEF1* promoter, considered one of the strongest promoters in yeast [38], was used in the remaining work. The impaired growth observed on carboxylic acids could be due to the reduction of intracellular citrate levels associated with the activity of CexA. Citrate secretion was observed in cells expressing CexA cultivated in liquid media containing acetic acid as the sole carbon source, whereas no citrate was detected in cultivations of cells transformed with the empty vector (Table 3). A similar behaviour was found in glucose-grown cells. Furthermore, and in accordance with previous studies [6], a decreased specific growth rate and final OD were observed in cells expressing CexA (Table 3) when compared to cells transformed with the empty plasmid.

The uptake rate of ^{14}C-citric acid (1.0 mM, pH 5.5) when CexA was expressed under the control of the *TEF1* promoter was 20 % higher than when CexA was expressed under the control of the *TPI1* promoter (not shown). The higher activity of CexA expressed under the control of the *TEF1* promoter is in accordance with the data presented in previous work [6], as well as with the growth phenotype observed on the drop tests (Fig. 1 A). Cells expressing CexA presented a first order kinetics for ^{14}C-citric acid uptake at pH 7.0 (Fig. 1 B), with higher velocities than cells transformed with the empty plasmid. At pH 5.5, cells expressing CexA presented saturable kinetics with the following estimated parameters: K_m 43.7 ± 13.4 mM of citric acid and V_{max} 9.4 ± 4.0 nmol citric acid s^{-1} mg^{-1} dry wt. (Fig. 1 C). A first order kinetics and lower velocities were found in cells transformed with the empty plasmid at both pH values. These findings suggest that CexA behaves as a citrate importer in *S. cerevisiae* and improves citric acid uptake. When assessing the effect of the pH (between pH 3.0 and pH 8.0) on the initial uptake rates of ^{14}C-citric acid in cells expressing CexA, we verified that the highest uptake occurred at pH 7.0 (Fig. 1 D). Citric and isocitric acids, but not monocarboxylic (acetate, lactate) or dicarboxylic acids (succinate, malate, α-ketoglutarate), were able to inhibit the uptake of labelled citric acid, suggesting that only tricarboxylates are able to bind to CexA (Fig. 1 E, F). The disruption of the proton motive force by the protonophore carbonyl cyanide m-chlorophenylhydrazone (CCCP), did not affect ^{14}C-citric acid transport, evidencing that CexA activity is independent of the proton motive force (Fig. 1 E).

3.2. Evolutionary relationships of CexA

Phylogenetic analysis was used to address the evolution of CexA homologs, which are members of the Drug-H^+ antiporter (DHA1) family (TC 2.A.1.2). A total of 580 hits were retrieved following a BLASTP screening against the NCBI's assembly database of complete genomes. Twenty-one hits were subsequently excluded due to sequence incompleteness in the highly conserved regions that characterize the gene family. The final dataset thus contained 559 sequences. All the homologs and corresponding bootstrap values from the CexA phylogenetic reconstruction are presented in Fig. S1. The phylogenetic tree of the DHA1 family (Fig. 2 A) presents homologs in eukaryotic organisms, divided into 5 clades (E1-E5), in addition to a single prokaryotic homolog from *Bacillus anthracis* (P1). CexA homologs were observed in several ascomycetes (orange) and in a smaller number of basidiomycetes members (brown), both distributed through the phylogenetic tree. Analysis targeting the *A. niger* CBS 513.88 strain highlighted sixteen proteins homologous to CexA (6 in the E1 clade, 8 in the E2, 2 in the E3 and 1 in the E4). The E1 clade contained ascomycetes and basidiomycetes homologs, including the CexA from *A. niger* [6], the itaconate transporter Itp1 from *Ustilago maydis* [9], the YALI0F03751g from *Yarrowia lipolytica* [16], and the multidrug transporters Qdr1 [39], Qdr2 [40] and Aqr1 [41,42] from *S. cerevisiae*. CexA was phylogenetically closer to homologs belonging to *Fusarium* species (*F. fujikuroi* and *F. oxysporum*), *Colletotrichum higginsianum*, *Neurospora crassa*, *Sclerotinia sclerotiorum*, *Botrytis cinerea*, *Penicillium chrysogenum*, and to one homolog from *Aspergillus oryzae*. The E2 clade included homologs found in *Y. lipolytica* that are not citrate

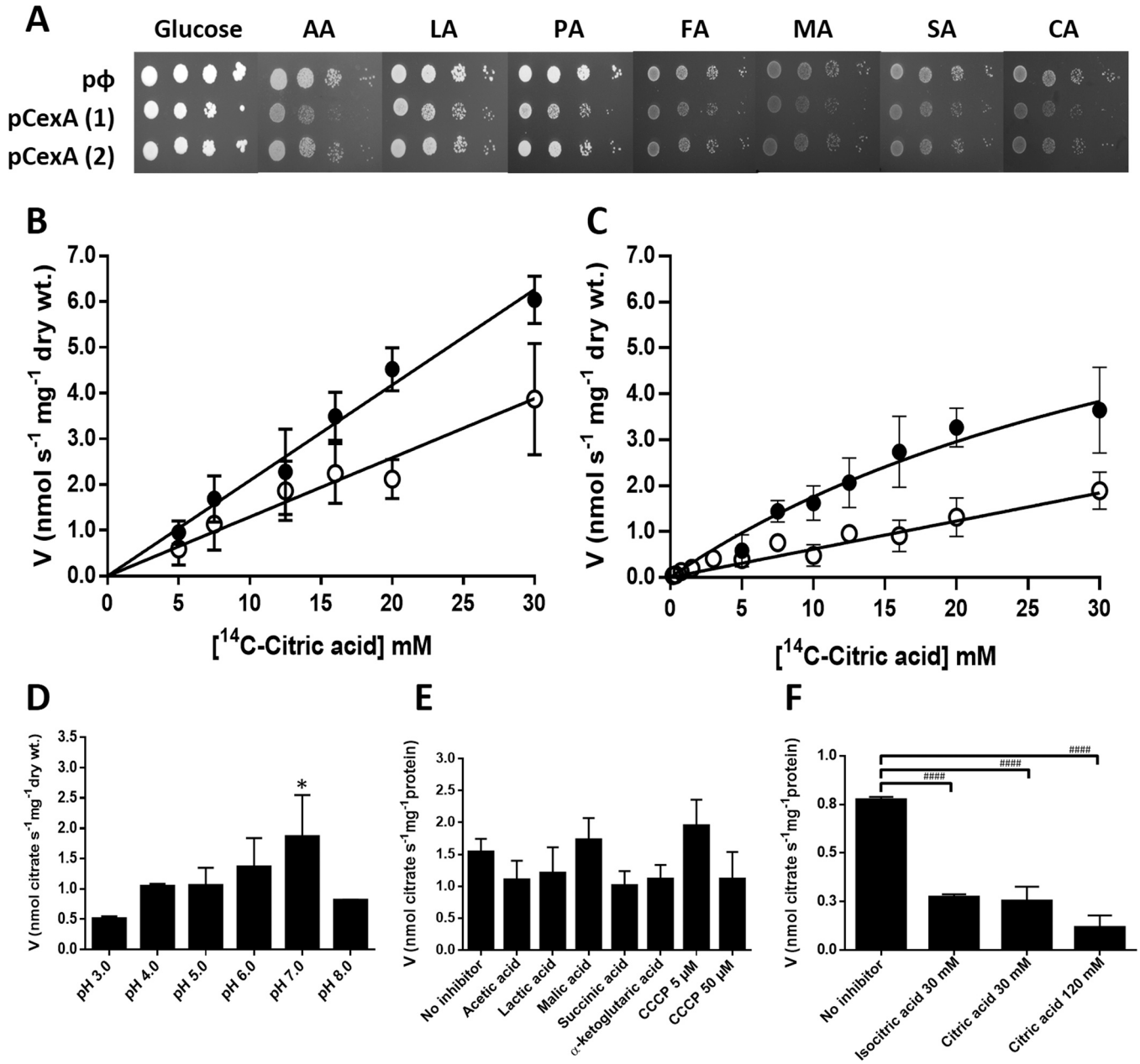

Fig. 1. Functional assays of *S. cerevisiae* CEN.PK 113–5D cells expressing the CexA transporter. A) Growth phenotype of cells transformed with the empty vector (pϕ), or expressing CexA under the control of promoter *TEF1* (pCexA-1) and *TPI1* (pCexA-2) on glucose, 2.0 % w/v, acetic acid, 0.5 % v/v, pH 6.0 (AA), lactic acid, 0.5 % v/v, pH 5.0 (LA), pyruvic acid, 0.5 % w/v, pH 5.0 (PA), fumaric acid, 1.0 % w/v, pH 5.0 (FA), malic acid, 1.0 % w/v, pH 5.0 (MA), succinic acid, 1.0 % w/v, pH 5.0 (SA) or citric acid, 1.0 % w/v, pH 5.5 (CA), as sole carbon sources, at 30 °C for 4 days. B) Initial uptake rates of ^{14}C-citric acid, pH 7.0, as a function of the acid concentration, in glucose-grown cells of *S. cerevisiae* cells transformed with pCexA-1(•) and with the empty plasmid pϕ (○). C) Initial uptake rates of ^{14}C-citric acid at pH 5.5 as a function of the acid concentration in glucose-grown cells of *S. cerevisiae* cells transformed with pCexA-1 (•) and with the empty plasmid pϕ (○). D) Effect of the pH on the transport of ^{14}C-citric acid, 10.0 mM, in glucose-grown cells of *S. cerevisiae* pCexA-1. E) ^{14}C-citric acid (12.0 mM, pH 5.5) uptake by glucose-grown cells of *S. cerevisiae* pCexA-1, in the absence or presence of non-labelled carboxylic acids (120 mM), or in the presence of CCCP. F) Transport of ^{14}C-citric acid 3.0 mM, pH 5.5, in glucose-grown cells of *S. cerevisiae* pCexA-1 in the absence or presence of non-labelled citric (30.0 mM and 120.0 mM) and isocitric (30.0 mM) acid. The data presented are mean values of at least three independent assays; the error bars represent the standard deviation. Statistical significance was estimated by one-way ANOVA followed by a post hoc Tukey's multiple comparisons test as follows: $^{*}P < 0.01$, pH 3.0 significantly different from pH 7.0; $^{\#\#\#\#}P < 0.0001$.

exporters [16], also proteins from *U. maydis* and other basidiomycetes such as *Cryptococcus*, *Sporisorium*, *Phellinus* and *Malassezia*, and several homologs belonging to other fungi. In the E3 clade, the sole characterized member was the *S. cerevisiae* multidrug transporter Qdr3 [43]. The E4 clade included two other *Y. lipolytica* homologs also reported as not being involved in citrate production [16]. The E5 clade contained Dtr1p, a putative dityrosine transporter from *S. cerevisiae* [44]. The alignment of all retrieved proteins present in the phylogenetic tree revealed several highly-conserved residues across all taxa (Fig. 2 B).

3.3. Site-directed mutagenesis of CexA

The predicted topology for CexA is presented in Fig. 3 A. CexA has 524 amino acid residues and 12 transmembrane segments (TMS). A total of 21 amino acid residues were selected for site-directed mutagenesis of CexA, taking into account the highly-conserved residues of the DHA1 family and predicted interactions with the substrate. The 3D model of CexA was obtained based on the structure of the L-lactate transporter from *Syntrophobacter fumaroxidans* (PDB 6G9X). This structure was the top-ranked template threading identified by

Table 3
Growth rate (k_c), final OD_{640} and citrate production of *S. cerevisiae* CEN.PK 113–5D transformed with pΦ or pCexA in YNB with either glucose (2 % w/v) or acetic acid (0.5 % v/v, pH 6.0) as carbon sources, supplemented with adequate requirements for prototrophic growth.

	Carbon source					
	Glucose			Acetic Acid		
Strains	k_c	Final OD_{640}[1]	[Citrate][2]	k_c	Final OD_{640}[1]	[Citrate][2]
pΦ	0.29 ± 0.01	1.8	Not Detected	0.10 ± 0.01	0.6	Not Detected
pCexA	0.22 ± 0.01	1.2	32.7 ± 10.1	0.03 ± 0.02	0.4	50.2 ± 1.0

(1) Final OD_{640} was measured at 12 h and 28 h in cell cultures containing glucose and acetic acid, respectively.
(2) The supernatant citrate concentration (mg/L) was evaluated in the time points indicated for the final OD_{640}.
The data presented are mean values plus SD of three independent assays.

HHpred (probability 100 %; e-value 4.9 e^{-35}; score 293.9). This carboxylic acid transporter is a member of the Major Facilitator Superfamily (MFS), with 12 TMS, a 14 % protein sequence identity with CexA, and an e-value of 3.7 e^{-35} in the BLASTP analysis. The highly conserved residues of the DHA1 family targeted for mutagenesis were G122, R123, R124, R154, P235, E236, T237 and R461. Molecular docking studies disclosed four binding regions for citrate on CexA (Fig. 3 B), revealing residues with strong interactions with citrate: P80, D84, P200, T207 (position 1), S75, N76, R192, Q196, Y307, S311, S315 (position 2), F188, R192, Y307, (position 3), S71, and R192 (position 4). The amino acid residues targeted for site-directed mutagenesis (replaced by an alanine), are highlighted both in Fig. 2 B (orange arrows and boxes) and in Fig. 3 A (grey dots).

3.4. Unveiling critical residues for citrate transport activity

The growth phenotype of *S. cerevisiae* CEN.PK 113–5D cells expressing the 21 *CexA* mutant alleles under the control of the *TEF1* promoter was evaluated in spot assays using distinct carbon sources (Fig. 4 A). Cells expressing the N76A and D84A mutant alleles revealed a growth profile similar to cells expressing the wild-type *CexA* allele on minimal media containing citric acid, indicating that these substitutions had no significant impact on protein activity. The mutant alleles S71A, S75A, P80A, G122A, R123 A, R124, R154, F188A, Q196A, T207A, P235A, E236A, S311A displayed the ability to use citric acid, showing an intermediate growth phenotype between cells transformed with pϕ and cells transformed with pCexA. As for the R192A, P200A, T237A, Y307A, S315A and R461A mutant alleles, a growth pattern similar to cells transformed with pϕ was obtained, suggesting that these residues are critical for citrate transport. For the remaining carboxylic acids, some variations in growth phenotypes were found for mutant alleles R124 A, R154A, Q196A, P200A, P235A, and S315A. A GFP C-terminal tagged version of the CexA alleles was constructed to determine whether the altered growth phenotypes were due to the mislocalization of the transporter. Epifluorescence microscopy analysis revealed that the mutant alleles S71A, G122A, R123A, R124A, R154A, E236A and T237A were not properly located at the plasma membrane, or presented low expression levels (Fig. 4 B). With exception of the residues S71 and R154, predicted to be located in TMS I and IV, respectively, residues G122, R123, R124, E236, and T237 are predicted to be located in transmembrane loops (Fig. 3 A).

The capacity to transport citrate was evaluated in the strains presenting proper localization at the plasma membrane of GFP-tagged CexA variants (Fig. 4 A). Reduced transport activity was observed for F188A, T207A, and P235A mutant alleles, whereas citrate uptake of the P200A, Y307A, S311A, S315A, and R461A variants was similar to the negative control. Cells expressing the N76A allele presented a citrate uptake rate similar to cells expressing CexA, whereas cells expressing the S75A, P80A, R192A and Q196A alleles showed higher citrate uptake rates. Fig. 4 C incorporates a summary table of the 12 mutant alleles properly located at the plasma membrane that displayed altered growth on citrate and/or citrate transport.

3.5. Kinetics of citrate import of the mutant alleles S75A, P80A, R192A and Q196A

The initial uptake rates of citrate were determined in the four mutant alleles displaying citrate transport activity higher than wild-type CexA. The kinetic parameters for ^{14}C-citric acid uptake at pH 5.5 of mutant allele S75A were K_m 11.8 ± 3.6 mM and V_{max} 5.6 ± 0.8 nmol s^{-1} mg^{-1} dry wt, revealing higher affinity for citrate than the values estimated for CexA (Fig. 5 A, B). Conversely, the kinetic parameters estimated for P80A (V_{max} 8.0 ± 2.9 nmol s^{-1} mg^{-1} dry wt; K_m 30.1 ± 17.4 mM), R192A (V_{max} 8.5 ± 2.1 nmol s^{-1} mg^{-1} dry wt, K_m 41.4 ± 14.8 mM) and Q196A (15.1 ± 4.4 nmol s^{-1} mg^{-1} dry wt, K_m 55.6 ± 21.8 mM) alleles were not statistically different to the ones estimated for the wild-type allele (Fig. 5 A, B). Despite the absence of relevant alterations in the import of citric acid, these mutant alleles displayed the ability to grow on citrate, a phenotype associated with an alteration of CexA transporter properties. The most striking phenotype was found in mutant R192A, which was able to grow on citrate much like cells transformed with the pϕ, but displayed activity for citrate import equivalent to cells transformed with the pCexA. The mutant alleles S75A, P80A, and Q196A revealed an intermediate growth on citrate and a citrate import similar to the wild-type CexA. A higher affinity for citrate import was found for the mutant S75A.

3.6. Export capacity of the mutant alleles S75A, P80A, R192A and Q196A

The phenotypes found for the mutant alleles S75A, P80A, R192A and Q196A, led us to hypothesize that the export of citric acid could be affected. The *Y. lipolytica* DSM 3286 strain deleted in Cex1 was used to express the CexA alleles under conditions similar to industrial fermentation, in order to evaluate the production of relevant metabolites (Fig. 6). All strains behaved similarly for biomass production and glycerol consumption. Besides citrate, α-ketoglutarate, erythritol, arabitol and mannitol were measured in the extracellular medium over time. The only significant differences compared to the expression of CexA were found in mutant alleles R192A and Q196A. Cells expressing the R192A allele produced residual levels of citrate (equivalent to the pattern observed for the strain transformed with the empty plasmid) and increased production of α-ketoglutarate. Regarding the mutant Q196A, a lower citrate and a higher α-ketoglutarate production were found.

3.7. Structure prediction of the mutant alleles

The pore topology prediction performed for mutant alleles mentioned in Fig. 4 C, detected significant alterations for the residues F188 (TMS V), R192 (TMS V) and Y307 (TMS VII) in comparison to the wild-type CexA. As depicted in Fig. 7 A, the most relevant alterations in the pore radius were located in the protein moiety

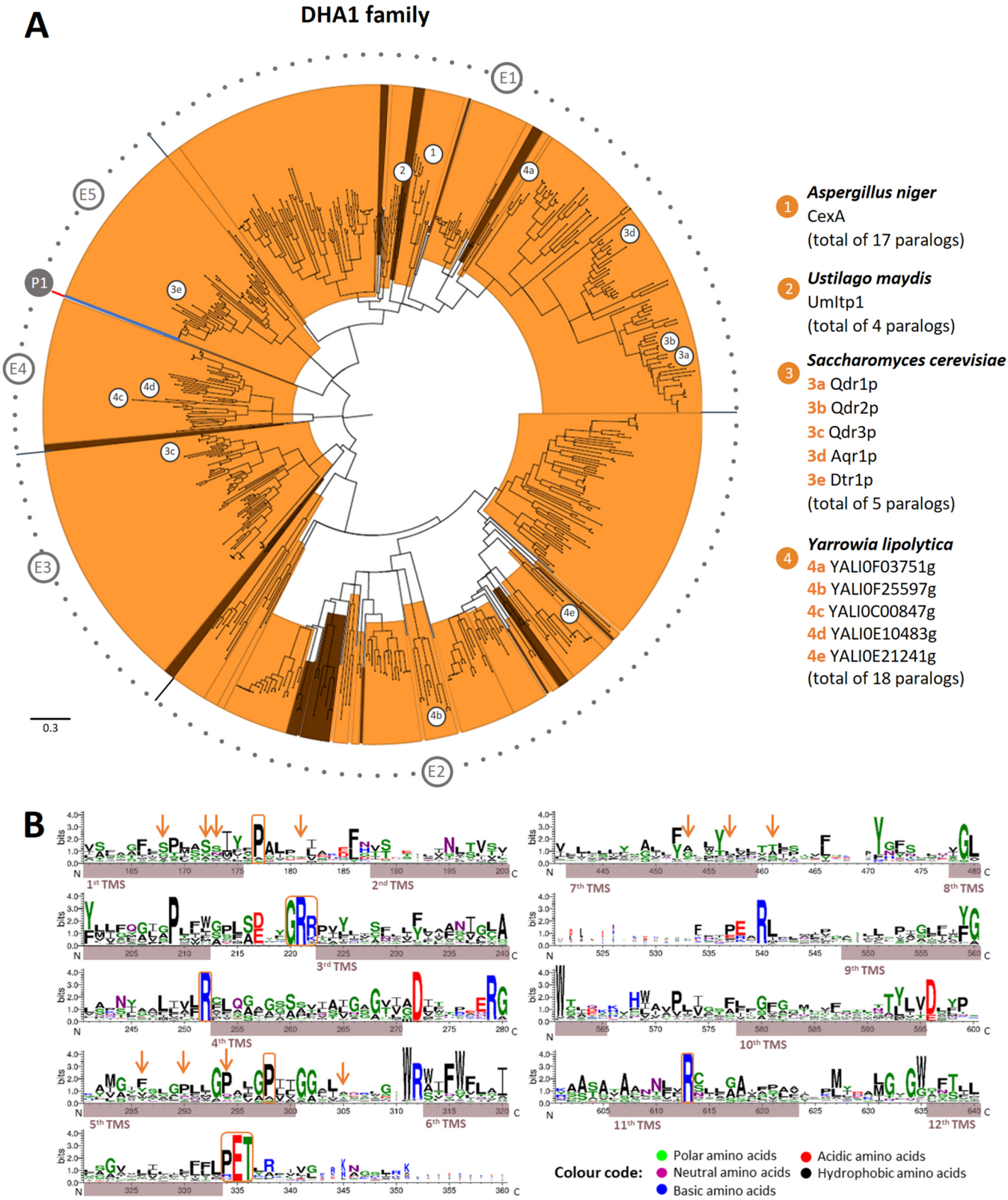

Fig. 2. Analysis of CexA homologs. A) Maximum likelihood phylogenetic tree of the DHA1 transporter family (TC#2.A.1.2). Branch lengths are proportional to sequence divergence. To facilitate the tree analysis the E1, E2, E3, E4, E5, and P1 groups were created which do not represent any type of classification. Colours represent the major taxonomic groups: bacteria (blue), ascomycetes (orange) and basidiomycetes (brown). The most relevant homologs discussed in the main text are highlighted in the figure. B) Partial representation of the conservation logo generated from the alignment of CexA homologs using WebLogo (https://weblogo.berkeley.edu), highlighting the relevant regions containing the amino acids targeted for mutagenesis. Sequences were used if they contained more than 90 % of aligned residues. Transmembrane segments (TMSs) are highlighted as brown bars in the logo. Orange arrows and boxes (highly conserved) indicate the 21 amino acids targeted for mutagenesis. The N- and C-terminal directions of the protein are indicated as N and C, respectively. (For interpretation of the references to colour in this figure legend, the reader is referred to the web version of this article.)

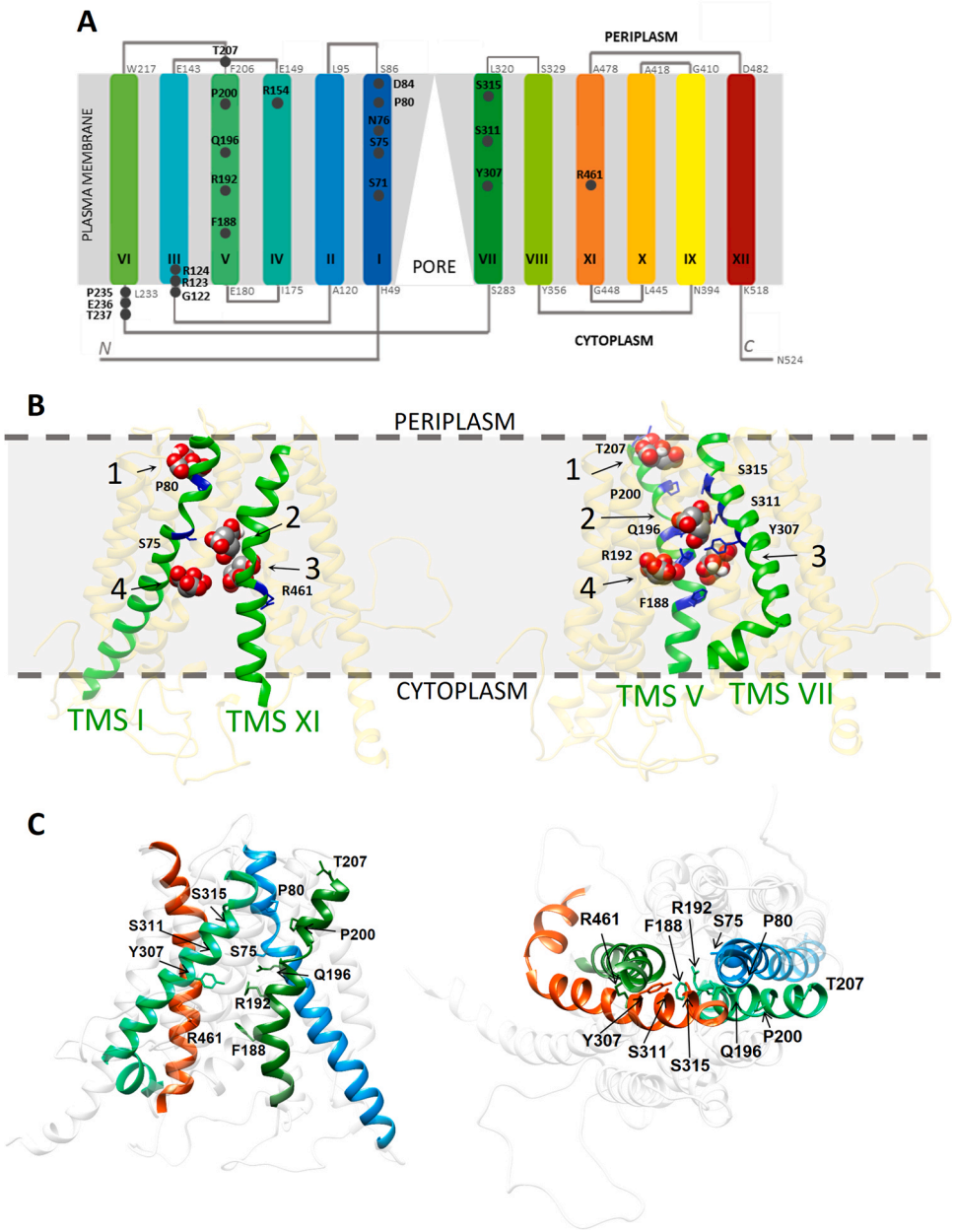

Fig. 3. Predicted structure of CexA transporter. A) Predicted topology of CexA with transmembrane segments (TMSs) coloured with the rainbow scheme from I to XII. The amino acid residues replaced by alanine are shown as grey circles: TMS I (S71, S75, N76, P80, D84), extracellular loop between TMS II and TMS III (G122, R123, R124), extracellular loop between TMS III and TMS IV (R154), TMS V (F188, R192, Q196, P200), extracellular loop between TMS V and TMS VI (T207), extracellular loop between TMS VI and TMS VII (P235, E236, T237), TMS VII (Y307, S311) extracellular loop between TMS VII and VIII (S315) and TMS XI (R461). The white triangle represents the central pore of the transporter. The N- and C-terminal directions of the protein are indicated as N and C, respectively. B) Transversal view of the CexA 3D model obtained by homology threading based on the crystal structure of the MFS transporter from *Syntrophobacter fumaroxidans* (PDB 6G9X). The residues interacting with citrate (red/grey colour) are located in TMS I, V, VII and XI. Four citrate-binding positions (1–4) were predicted by molecular docking. C) Top and side view of the central pore of the 3D-model of CexA highlighting amino acid residues S75, P80, F188, R192, Q196, P200, T207, Y307, S311, S315, and R461, predicted to be part of the substrate translocation pathway (For interpretation of the references to colour in this figure legend, the reader is referred to the web version of this article.).

facing the cytoplasm, between positions − 15 and − 5 on the pore axis. In the R192A mutant allele, the pore radius increased from 1.6 Å to 3.9 Å around position − 10 (see arrow in Fig. 7 B). The widening of pore radius around position − 10 was also found in the Y307A mutant allele, although to a lesser extent (see arrow in Fig. 7 B). The F188A substitution caused not only a widening of the pore in the same position, but also a narrowing of the radius near the position − 5, from 3.2 Å to 1.1 Å (see arrow in Fig. 7 B).

Docking analysis with the HHpred CexA model revealed that the F188 residue interacts with citrate in binding position 3, whereas Y307 interacts with citrate in binding positions 2 and 3. In accordance, the functional analysis supported the involvement of residues F188 and Y307 in the translocation pathway of citrate. The R192, with a key role in the export of the acid, is the sole residue presenting salt bridge interactions in the binding positions 2, 3 and 4. An example of these interactions is presented in Fig. 7 C, showing the predicted molecular interactions of the R192 residue in position 2 with the three anionic forms of citrate. The Q196 residue, relevant for citrate export and also located in TMS V, only interacts with citrate in position 2 (Fig. 3 B). Likewise, the residue S75 (TMS I)

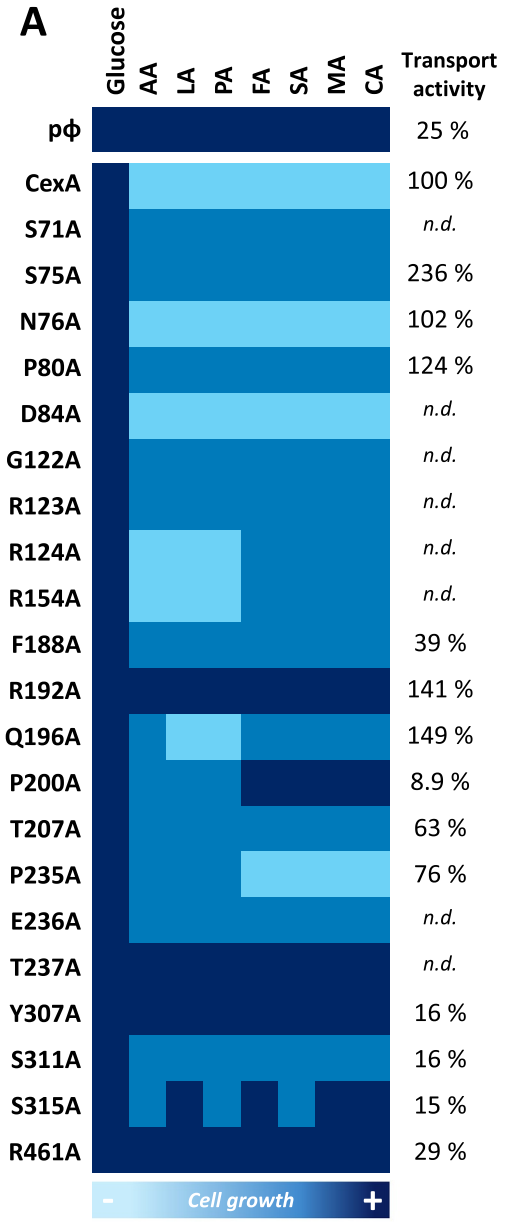

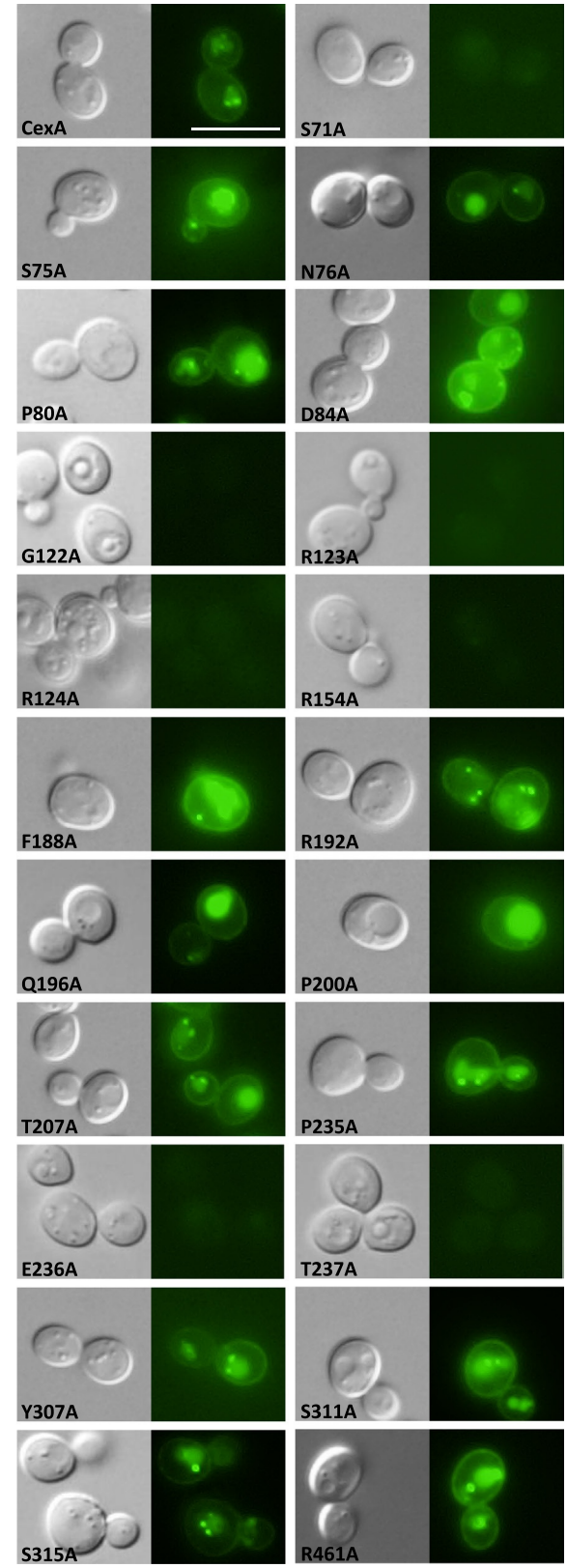

C

Transport activity	Growth on citrate: Intermediate	Growth on citrate: pϕ
>100%	S75A, Q196A, P80A	R192A
~50%	F188A, T207A, P235A	-
<30%	S311A	P200A, Y307A, S315A, R461A

(caption on next page)

Fig. 4. Characterization of CexA mutant alleles expressed in *S. cerevisiae* CEN.PK 113–5D. A) Heatmap of CexA mutant alleles according to their ability to grow in media containing glucose, 2.0 % w/v, acetic acid, 0.5 % v/v, pH 6.0 (AA), lactic acid, 0.5 % v/v, pH 5.0 (LA), pyruvic acid, 0.5 % w/v, pH 5.0 (PA), fumaric acid, 1.0 % w/v, pH 5.0 (FA), malic acid, 1.0 % w/v, pH 5.0 (MA), succinic acid, 1.0 % w/v, pH 5.0 (SA) or citric acid, 1.0 % w/v, pH 5.5 (CA), as sole carbon sources, at 30 °C for 4 days. Transport activity was determined in glucose-grown cells with ^{14}C-citric acid, 10.0 mM, pH 5.5, assuming as 100 % the initial uptake rate of the wild-type CexA. The cells transformed with the empty vector are represented by pϕ. The abbreviation n.d. stands for not determined. B) Localization of GFP-tagged CexA and mutant alleles in glucose grown-cells observed by epifluorescence microscopy. C) Summary table of the phenotype of 12 CexA mutant alleles expressed in *S. cerevisiae* properly localized at the plasma membrane. Two categories were considered for growth on citric acid: cells displaying full growth on citric acid (similar to pϕ); cells showing an intermediate phenotype, higher than pCexA and lower than pϕ. Three categories were considered for the uptake of citric acid: higher than CexA (100 %), approximately 50 % and less than 30 %. The predicted location of the corresponding amino acid residues is presented in Fig. 3 B, C.

interacts with citrate in binding position 2 and its substitution to alanine increased the affinity of citrate uptake.

According to the CexA predicted structure, the TMS I, V, VII and XI (Fig. 3 C) form the central pore of the transporter. Supporting this model is the loss of function, both in the import and export of citrate, observed for mutations in residues P200 (TMS V), Y307 (TMS VII), S315 (TMS VII) and R461 (TMS XI). Although undetected initially with the HHpred CexA model, molecular interactions of the conserved R416 residue with citrate were found when AlphaFold was used (not shown). The results obtained with the two structural prediction bioinformatics tools complemented each other, and brought robustness to the CexA structural 3D model herein described. Nevertheless, functional assays are needed to confirm modelling approaches. For instance, the residues S71, P80, F188, T207 and S311 were only predicted to interact with citrate in the HHpred model. Conversely, the conserved residue R123 was only found to interact with citrate when using the AlphaFold model.

4. Discussion

4.1. Heterologous expression of CexA in Saccharomyces cerevisiae

The heterologous expression of *CexA,* under the control of a constitutive promoter, impaired *Saccharomyces cerevisiae* cell growth in minimal media containing carboxylic acids (Fig. 1). We postulate that this phenotype is due to the secretion of citrate to the extracellular media (Table 3), associated with the expression of CexA, which depletes the cells of citrate, a substrate of the citric acid cycle crucial to support cell metabolism in respiratory substrates. It has been shown that constitutive expression of CexA in *Aspergillus niger* decreases conidiation patterns when grown in solid media [6]. Therefore, we cannot exclude that the expression of *CexA* in *S. cerevisiae* may also interfere with other cellular traits.

CexA activity is influenced by the pH (Fig. 1 B, C, D). An increase in citrate uptake occurred above the pK_{a1} of citrate (pK_{a1}=3.13; pK_{a2}=4.76; pK_{a3}=6.40) [4] suggesting that charged forms of citrate

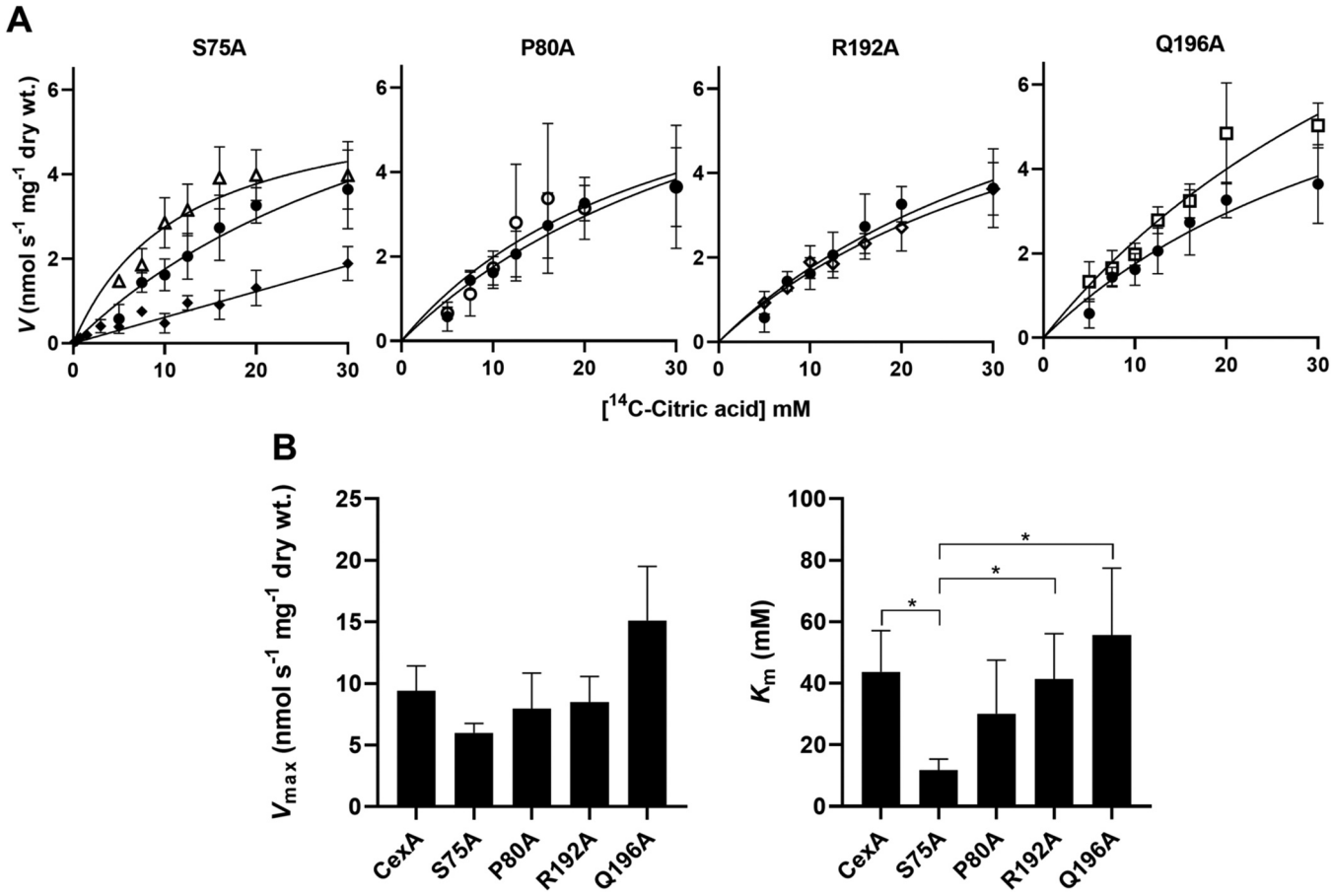

Fig. 5. Transport of ^{14}C-citric acid at pH 5.5 in *S. cerevisiae* CEN.PK 113–5D cells expressing the S75A, P80A, R192A and Q196A CexA mutant alleles. A) Initial uptake rates of ^{14}C-citric acid as a function of the acid concentration in glucose-grown cells transformed with plasmids pϕ (◆), pCexA (•), pCexA-S75A (Δ), pCexA-P80A (○), pCexA-R192A (◊) and pCexA-Q196A (□). The data shown are mean values of at least three independent experiments and the error bars represent the standard deviation. B) Kinetic parameters, V_{max} and $K_{m,}$ for ^{14}C-citric acid uptake estimated from the plots presented in A). Error bars correspond to the SE (* $P < 0.05$). An unpaired *t*-test was done for the evaluation of significant differences.

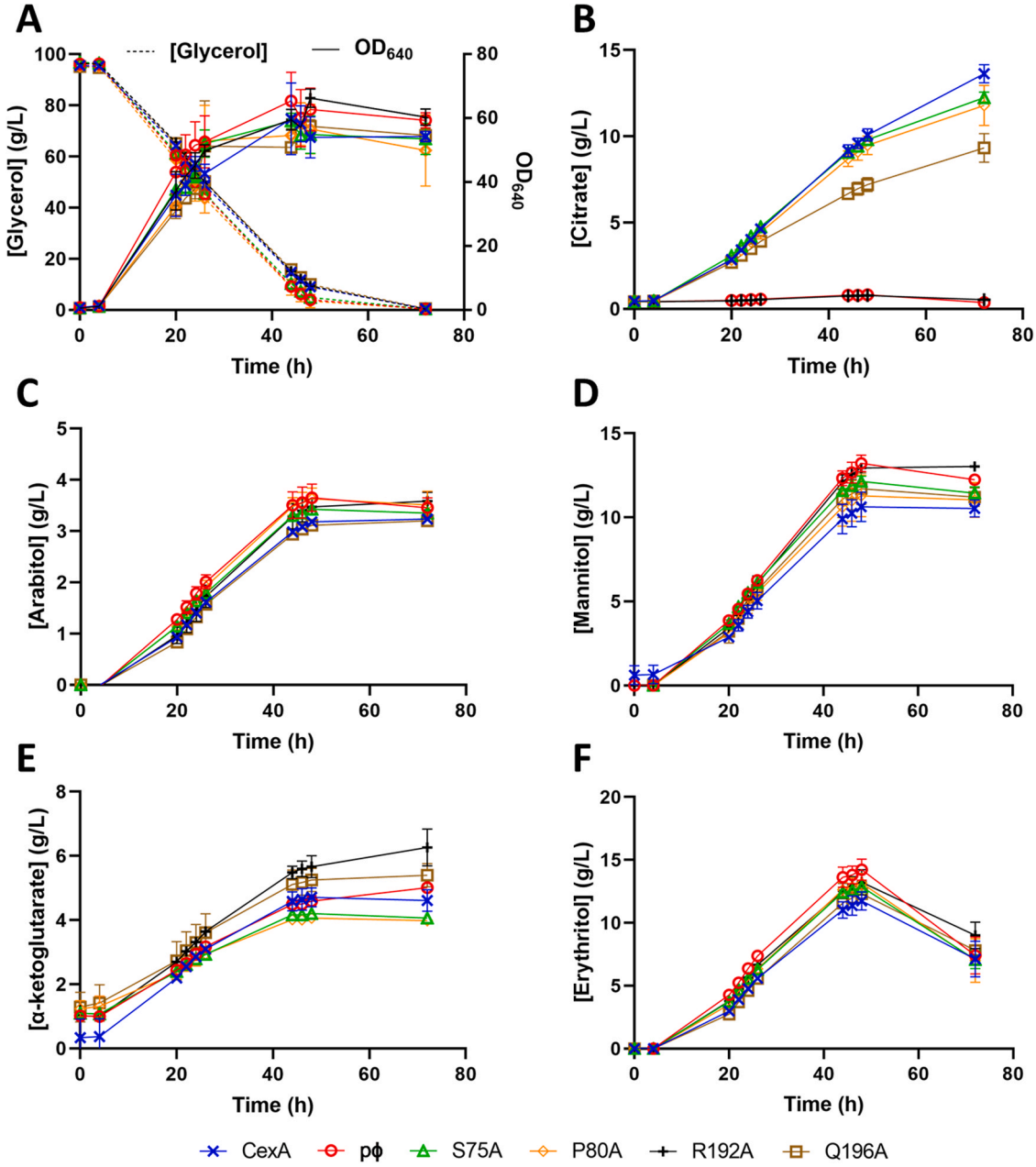

Fig. 6. Cultivation of *Yarrowia lipolytica* DSM *3286 Cex1*Δ on glycerol, 100 g/L, pH 5.5. The distinct strains express the wild-type CexA (×), the mutant alleles S75A (△), P80A (◇), R192A (+), Q196A (□), and cells transformed with the empty vector (○). (A) Cell culture growth and glycerol consumption; production of (B) citrate, (C) arabitol, (D) mannitol, (E) α-ketoglutarate, and (F) erythritol. An HPLC analysis was used to determine the concentration of metabolites present in the culture supernatants. Biomass accumulation was measured by optical density at 640 nm (OD_{640}). A detailed description of culture conditions can be found in the Materials and Methods section. Mean values and standard deviations were determined from three biological replicates and an unpaired *t*-test was done for evaluation of significant differences.

are transported by *CexA*. When the pH is lower than the pK_{a1} of the citric acid, the undissociated form predominates, being able to enter the cell by simple diffusion [45]. At a pH value higher than the pK_{a1} of citric acid, the charged anionic forms prevail, requiring a transporter protein in order to cross the plasma membrane [45]. The reduction in the citrate uptake observed at pH 8.0 is in agreement with previous studies, indicating that this is a critical and non-physiological pH value for *S. cerevisiae* cells [46]. The uptake of citrate was higher at pH 7.0 (Fig. 1 D), displaying linear kinetics for the initial uptake rates of citrate as a function of citrate concentration (Fig. 1 B). At this pH, citric acid is in the fully deprotonated state ($pH > pK_{a3}$) reinforcing the evidence that the anionic form(s) of the acid is the substrate of CexA. At pH 5.5, the estimated kinetic parameters for citrate uptake are in agreement with a low-affinity and high-capacity transporter. Further studies analysing the uptake of citrate at different pH are necessary to disclose which anionic form of citrate is preferentially transported by CexA. The outcome of the protonophore CCCP on citrate uptake evidenced the independence of the CexA transporter from the proton motive force (Fig. 1 E), excluding the hypothesis of CexA acting as a secondary active transporter [6], but rather as a passive transport mechanism [45]. Furthermore, the kinetics at pH 7.0 and 5.5 (Fig. 1 B, C) are compatible with a mediated mechanism for citrate transport through a facilitated diffusion [45], and are in accordance with its primary role as an exporter. To be an efficient exporter, the transporter needs to have a low affinity for substrate import, hence avoiding a futile cycle. Previous works have reported carboxylic acid exporters as low-affinity transport systems. An example of such

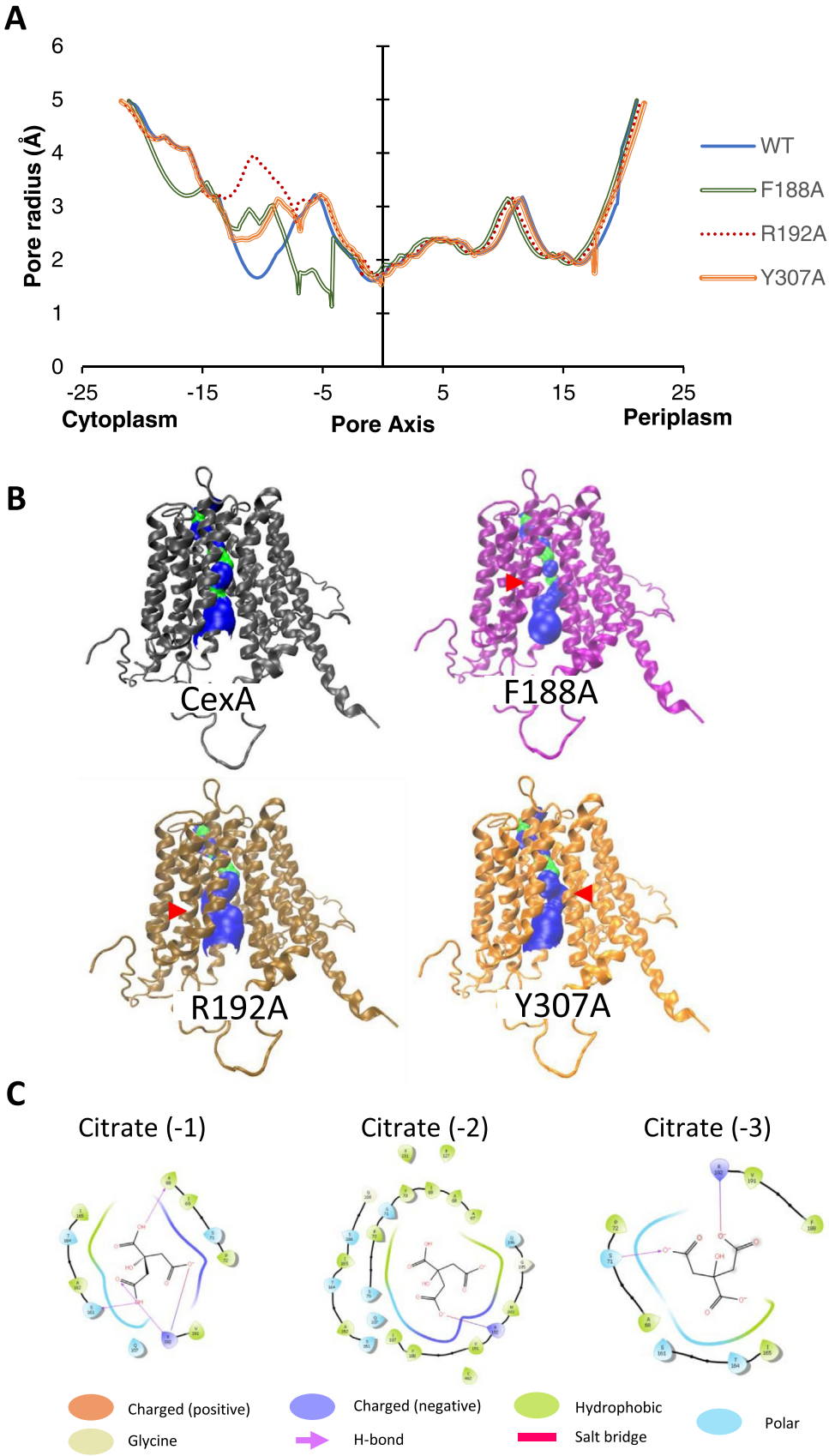

Fig. 7. Pore topology prediction of the CexA transporter. A) Prediction of the pore radius plotted along the axis of CexA and mutations F188A, R192A, and Y307A using the HOLE software. B) Analysis of the effect of the F188A, R192A and Y307A mutations on the predicted transporter 3D structure. The arrow highlights the location of the F188, R192 and Y307 positions. Solid surface representation of the intraprotein radius variation is depicted in blue (larger aperture) and green (more constricted). C) Representation of CexA 2D view, with the interactions predicted by molecular docking. The R192 residue displays strong molecular interactions (salt bridges) with citrate^{-1}, citrate^{-2}, and citrate^{-3} in position 4. The images were obtained with the Maestro Schrödinger Software.

physiological behaviour is present in human cells where the low-affinity plasma membrane monocarboxylate transporter MCT4 is mostly associated with the export, whereas the homologue MCT1, a high-affinity monocarboxylate transporter, is typically associated with the import of the acids [47]. Several citrate transporters have been found in fungi species. The first report was described in the 90 s in *Candida utilis* where low- and high-affinity transport systems for citrate transport were characterized [48,49]. Furthermore, other citrate transporters have been characterized. However, the kinetic parameters for citrate transporters were not reported, namely, for *An*Best1, an anion efflux channel from *Aspergillus nidulans* [50], for *Yl*Cex1 from *Y. lipolytica* [16], and *Pk*JEN2–2 from *Pichia kudriavzevii* [51]. A recent study in the yeast *Cyberlindnera jadinii* [52] identified the citrate transporters *Cj*Ato5, *Cj*Jen6, and *Cj*Slc5, reporting K_m values for the uptake of citrate of 21.2, 21.4 and 17.2 mM, respectively.

4.2. Phylogeny of CexA

So far, the CexA transporter is the sole member of the DHA1 transporter family to be functionally characterized as a citrate transporter, despite the fact that this family has a high occurrence in fungi (Fig. 2). The detection of a sole prokaryotic member in our phylogenetic investigation is likely due to a horizontal gene transfer event. The itaconate transporter Itp1p from *U. maydis* [9] and the multidrug transporters Qdr1, Qdr2, and Aqr1 from *S. cerevisiae* [39–42] are the only CexA homologs functionally characterized. Aqr1 is a carboxylic acid transporter that was reported to confer resistance to monocarboxylic acids and quinidine while being also involved in the secretion of amino acids [41,42]. The expression of Qdr1 promotes resistance to drugs like quinidine, ketoconazole, and fluconazole, and it intervenes in the spore wall assembly [39]. The Qdr2 transporter has a wide-ranging substrate specificity that includes numerous drugs and mono- and divalent cations, also promoting potassium homeostasis [40] and the export of copper [53]. Other members of the DHA1 family present in *S. cerevisiae*, such as Flr1, Hol1, Tpo1, Tpo2, Tpo3, Tpo4, and Yhk8, were not present in the phylogenetic tree since they failed to meet our stringency criteria due to a low identity with CexA [54]. Recent work reported the Tpo2 and Tpo3 transporters as the major acetate efflux systems in *S. cerevisiae*, and that Aqr1 only plays a minor role in this process [55]. In the yeast *Y. lipolytica,* the CexA homologs are not citrate exporters, and the function of these genes is still unknown, while the citrate exporter Cex1 is a member of the DHA2 transporter family [16]. An interesting aspect is that the number of CexA homologs seems to be strain dependent. In the genome of the *A. niger* ATCC 1015 strain, six homologs were identified, whereas in the genome of the reference strain CBS 513.88, seventeen homologs are annotated. A high genomic variation was reported for this species, supported by phylogenetic studies and exo-metabolite profiling [56]. Also, a larger number of transporters belonging to the MFS were identified in the genome of the *A. niger* CBS 513.88 strain [57]. Nonetheless, in these two strains the CexA protein sequence only varies in one residue I21T localized in the N-terminal region of the protein.

4.3. Structural-functional analysis of CexA

The CexA 3D-model structure was predicted with HHpred, using as a template an MFS lactate transporter from *Syntrophobacter fumaroxidans* belonging to the Solute Carrier member 16 (SLC16) family [31]. This family comprises several carboxylic acid transporters, namely the human proton-linked monocarboxylate transporters MCT1–4 [58]. Molecular docking studies of CexA revealed four putative citrate-binding sites, one facing the extracellular space (Fig. 3 B, position 1) and three in the central region of the protein (Fig. 3 B, positions 2–4). As shown in Fig. 3 B, TMS I, V, VII and XI contain the residues predicted to be involved in citric acid binding and in this study we disclose their functional role in citrate transport.

The amino acid residues conserved throughout evolution (Fig. 2 B; orange boxes) are mostly located in membrane loops. Substitutions in these amino acids, namely the ^{122}GRR^{124} R154, and ^{236}ET^{237}, impacted largely on the localization of the protein. The ^{122}GRR^{124} and ^{235}PET^{237} appear within two blocks of conserved residues in the amino acid sequence alignment of CexA homologues (Fig. 3 A), located at the beginning of TMS III and VI, respectively. In the predicted 3D structure of CexA, these two blocks are in proximity to each other, with the negatively charged side chain of the E236 in contact with the positive side chain of the R123 and R124 residues (not shown), indicating that these conserved residues have a structural function and, potentially, their substitution to alanine affects transporter conformation and correct trafficking to the plasma membrane. The CexA structure predicted by AlphaFold also evidenced the positioning of the ^{122}GRR^{124} facing the conserved block ^{235}PET^{237} (not shown), reinforcing the hypothesis that the interaction between these two conserved blocks has a role in protein conformation, contributing to the stability of the transporter. The P235A mutation did not affect protein localization at the plasma membrane (Fig. 4 B), but led to a decreased citrate transport capacity, an indication of its role in the proper function and structure of CexA. The amino acid S71 located in the middle of TMS I, albeit not being conserved, also hindered protein localization at the plasma membrane when substituted to alanine, and it most probably plays an important role in transporter conformation.

Combining the 3D models obtained with HHpred and AlphaFold with the functional analysis of the CexA mutant alleles evidenced amino acid residues that are part of the substrate translocation pathway (Fig. 3 C). They include the S75, N76, P80 (TMS I), F188, R192, Q196, P200, T207 (TMS V), Y307, S311, S315 (TMS VII) and R461 (TMS XI) residues. The four citrate-binding positions predicted by molecular docking using the HHpred model revealed the inward positioning of all the above-mentioned residues, facing the central pore. When using the AlphaFold model, these residues were also predicted to interact with citrate, except for P80, F188, P200, T207 and S311. Conversely, the AlphaFold model predicted a citrate interaction with the R123 residue, a feature not evidenced when using HHpred.

Some amino acid substitutions lead to the complete or partial loss of CexA activity. Mutations in the residues P200, Y307, S315, and R461 originated a loss of function of the transporter, resulting in improved growth on citrate. These results are indicative of their crucial role in substrate binding and translocation throughout the protein pore. The substitutions F188A, T207A, and S311A resulted in a partial loss-of-function, with altered growth phenotype on citrate. All of these residues were predicted to interact with citrate (Fig. 3 B) and are associated with the transport of citric acid.

The shortening of the side chain of the F188 and Y307 residues resulted in a widening of the pore radius (Fig. 7) which are located in binding positions 3 and 4. We hypothesize that the widening of the pore region facing the cytoplasm facilitates access to position 2, thus affecting both the import and the export of citrate.

The mutant alleles S75A, P80A, and Q196A present an intermediate growth phenotype on citrate. This result suggests that these substitutions cause a lower capacity to export citrate. The conserved non-polar residue P80 is located in binding position 1. The rigidity provided by the proline led us to postulate the importance of this residue for transport activity. We found that mutation of P80 lead to an altered growth phenotype on all carboxylic acids tested and an increased citrate uptake in *S. cerevisiae* (Fig. 4). However, the P80A substitution did not influence the production of citrate in *Y. lipolytica* (Fig. 6). The S75A substitution promoted a higher affinity for citrate import (Fig. 5) and higher cell growth on carboxylic acids. In this mutant, the export capacity was not affected, as citrate production in

Y. lipolytica was similar to cells expressing CexA. Thus, the decreased K_m for citrate was only affecting the import and did not affect the export of citrate. No significant differences in citrate uptake were found in cells expressing the Q196A (TMS V) mutant allele (Fig. 5). However, this mutant presented a diminished production of citrate (Fig. 6). Thus, Q196 is a key residue for citrate export.

Another residue critical for citrate translocation is the R192 (TMS V). Cells expressing the R192A mutant allele presented a growth phenotype similar to cells carrying the empty vector, while maintaining a citrate uptake similar to the wild-type CexA (Fig. 5). This suggests that such a substitution influences protein activity, maintaining the import of citrate but impairing the export. This hypothesis was confirmed in bioreactor cultivations where the production of citric acid equaled the profile of cells transformed with the empty vector (Fig. 6). The small increase in α-ketoglutarate production observed in *Y. lipolytica* cells expressing the R192A mutant allele can be due to the intracellular accumulation of citrate, leading to an increase of this intermediate compound of the TCA cycle, resulting in its secretion to the extracellular media (Fig. 6 E). As shown in Fig. 7, the R192A substitution promoted a strong alteration in the predicted pore radius for CexA, widening the pore in the proximity of the cytoplasm. Curiously, the R192 residue is not conserved throughout the evolution of the DHA1 family, but it is the sole CexA residue predicted to form a salt bridge with citrate (Fig. 7 C), suggesting the relevant role of this interaction for citrate export.

5. Conclusions

Tricarboxylic acids, including citric and isocitric acids, are chemical building blocks with an increasing demand in the global market due to their application in several industrial sectors. Filamentous fungi, and in particular *Aspergillus niger*, are crucial players in the microbial production of citric acid via fermentation [2]. Here, membrane transporter proteins play a critical role in the improvement of metabolite export, directly influencing microbial cell factory productivity. In the present work, we used heterologous expression in *Saccharomyces cerevisiae* to deepen the knowledge of the *A. niger* CexA citrate exporter. We uncovered its ability to also import citrate, although with low affinity. In addition, a combination of phylogenetic analysis, identification of conserved domains, 3D model prediction, molecular docking and site-directed mutagenesis allowed us to uncover structural features of CexA, including critical residues for protein function. Finally, the use of *Yarrowia lipolytica* allowed us to reveal CexA mutant alleles affecting citrate export. We uncovered the role of S75 on citrate import, as its substitution for alanine increased the affinity of the transporter for citrate. The most critical residues for citrate export were R192 and Q196, considering that their substitution for alanine altered the ability to produce citric acid in bioreactor fermentations. Ultimately, we disclosed key amino acid residues involved in citrate binding and translocation in CexA.

Funding

This work was supported by the Strategic Programme UID/BIA/04050/2020 and the project LA/P/0069/2020 granted to the Associate Laboratory ARNET, both funded by Portuguese funds through the FCT-IP. J.A. acknowledges the FCT and the Doctoral Program in Applied and Environmental Microbiology for the PD/BD/150584/2020 PhD grant and a COST Action CA18113 Short-Term Scientific Mission grant (EuroMicropH). M.S.S. acknowledges the Norte2020 for the UMINHO/BD/25/2016 PhD grant with the reference NORTE-08-5369-FSE-000060. I.S-S. was supported by the program contract FCTUMINHO/Norma transitória from the Legal Regime of Scientific Employment (RJEC).

CRediT authorship contribution statement

João Alves: Investigation, Visualization, Formal analysis, Writing – original draft. **Maria Sousa-Silva:** Investigation, Validation, Visualization, Writing – original draft. **Pedro Soares:** Investigation, Formal analysis, Writing – original draft. **Michael Sauer:** Supervision, Investigation, Writing – review & editing. **Margarida Casal:** Conceptualization, Investigation, Validation, Funding acquisition, Supervision, Writing – review & editing. **Isabel Soares-Silva:** Conceptualization, Investigation, Validation, Funding acquisition, Supervision, Writing – review & editing.

Conflict of interest

The authors declare that they have no conflict of interest.

Appendix A. Supporting information

Supplementary data associated with this article can be found in the online version at doi:10.1016/j.csbj.2023.04.025.

References

[1] Soares-Silva I, Ribas D, Sousa-Silva M, Azevedo-Silva J, Rendulić T, Casal M. Membrane transporters in the bioproduction of organic acids: state of the art and future perspectives for industrial applications. FEMS Microbiol Lett 2020;367(15). https://doi.org/10.1093/femsle/fnaa118
[2] Behera B, Mishra R, Mohapatra S. Microbial citric acid: production, properties, application, and future perspectives. Food Front 2021;2(1):62–76. https://doi.org/10.1002/fft2.66
[3] Analysts GI, Global Citric Acid Industry; 2020: p. 1-351.
[4] Show P, Oladele K, Siew Q, Aziz Zakry F, Lan J, Ling T. Overview of citric acid production from *Aspergillus niger*. Front Life Sci 2015;8(3):271–83. https://doi.org/10.1080/21553769.2015.1033653
[5] Parshikov I, Woodling K, Sutherland J. Biotransformations of organic compounds mediated by cultures of *Aspergillus niger*. Appl Microbiol Biotechnol 2015;99(17):6971–86. https://doi.org/10.1007/s00253-015-6765-0
[6] Steiger MG, Rassinger A, Mattanovich D, Sauer M. Engineering of the citrate exporter protein enables high citric acid production in *Aspergillus niger*. Metab Eng 2019;52:224–31. https://doi.org/10.1016/j.ymben.2018.12.004
[7] Sauer M. Membrane transport as a target for metabolic engineering. In: Joshi S, editor. Designer Microbial Cell Factories: Metabolic Engineering and Applications Elsevier; 2022. p. 27–43. https://doi.org/10.1016/B978-0-323-88504-1.00003-0
[8] Boyarskiy S, Tullman-Ercek D. Getting pumped: membrane efflux transporters for enhanced biomolecule production. Curr Opin Chem Biol 2015;28:15–9. https://doi.org/10.1016/j.cbpa.2015.05.019
[9] Geiser E, Przybilla S, Friedrich A, Buckel W, Wierckx N, Blank L, et al. *Ustilago maydis* produces itaconic acid via the unusual intermediate trans-aconitate. Microb Biotechnol 2016;9(1):116–26. https://doi.org/10.1111/1751-7915.12329
[10] Huang X, Lu X, Li Y, Li X, Li J-J. Improving itaconic acid production through genetic engineering of an industrial *Aspergillus terreus* strain. Microb Cell Factor 2014;13(1):119. https://doi.org/10.1186/s12934-014-0119-y
[11] Wierckx N, Agrimi G, Lübeck PS, Steiger MG, Mira NP, Punt PJ. Metabolic specialization in itaconic acid production: a tale of two fungi. Curr Opin Biotechnol 2020;62:153–9. https://doi.org/10.1016/j.copbio.2019.09.014
[12] Camarasa C, Bidard F, Bony M, Barre P, Dequin S. Characterization of *Schizosaccharomyces pombe* malate permease by expression in *Saccharomyces cerevisiae*. Appl Environ Microbiol 2001;67(9):4144–51. https://doi.org/10.1128/aem.67.9.4144-4151.2001
[13] Darbani B, Stovicek V, van der Hoek SA, Borodina I. Engineering energetically efficient transport of dicarboxylic acids in yeast *Saccharomyces cerevisiae*. Proc Natl Acad Sci USA 2019;116(39):19415–20. https://doi.org/10.1073/pnas.1900287116
[14] Pacheco A, Talaia G, Sá-Pessoa J, Bessa D, Gonçalves MJ, Moreira R, et al. Lactic acid production in *Saccharomyces cerevisiae* is modulated by expression of the monocarboxylate transporters Jen1 and Ady2. FEMS Yeast Res 2012;12(3):375–81. https://doi.org/10.1111/j.1567-1364.2012.00790.x
[15] Odoni D, Vazquez-Vilar M, van Gaal M, Schonewille T, Martins dos Santos V, Tamayo-Ramos J, et al. *Aspergillus niger* citrate exporter revealed by comparison of two alternative citrate producing conditions. FEMS Microbiol Lett 2019;366(7). https://doi.org/10.1093/femsle/fnz071
[16] Erian AM, Egermeier M, Rassinger A, Marx H, Sauer M. Identification of the citrate exporter Cex1 of *Yarrowia lipolytica*. FEMS Yeast Res 2020;20(7). https://doi.org/10.1093/femsyr/foaa055
[17] Nakamura E, Kadooka C, Okutsu K, Yoshizaki Y, Takamine K, Goto M, et al. Citrate exporter enhances both extracellular and intracellular citric acid accumulation in the koji fungi *Aspergillus luchuensis* mut. *kawachii* and *Aspergillus oryzae*. J Biosci Bioeng 2021;131(1):68–76. https://doi.org/10.1016/j.jbiosc.2020.09.002

[18] Papagianni M. Advances in citric acid fermentation by *Aspergillus niger*: biochemical aspects, membrane transport and modeling. Biotechnol Adv 2007;25(3):244–63. https://doi.org/10.1016/j.biotechadv.2007.01.002
[19] Entian K, Kötter P. 25 yeast genetic strain and plasmid collections. Methods Microbiol 2007;36:629–66. https://doi.org/10.1016/S0580-9517(06)36025-4
[20] Ribas D, Sá-Pessoa J, Soares-Silva I, Paiva S, Nygard Y, Ruohonen L, et al. Yeast as a tool to express sugar acid transporters with biotechnological interest. FEMS Yeast Res 2017;17(2). https://doi.org/10.1093/femsyr/fox005
[21] Soares-Silva I, Paiva S, Diallinas G, Casal M. The conserved sequence NXX [S/T] HX [S/T] QDXXXT of the lactate/pyruvate: H+ symporter subfamily defines the function of the substrate translocation pathway. Mol Membr Biol 2007;24(5–6):464–74. https://doi.org/10.1080/09687680701342669
[22] Egermeier M, Sauer M, Marx H. Golden Gate-based metabolic engineering strategy for wild-type strains of *Yarrowia lipolytica*. FEMS Microbiol Lett 2019;366(4). https://doi.org/10.1093/femsle/fnz022
[23] Ribas D, Soares-Silva I, Vieira D, Sousa-Silva M, Sá-Pessoa J, Azevedo-Silva J, et al. The acetate uptake transporter family motif "NPAPLGL (M/S)" is essential for substrate uptake. Fungal Genet Biol 2019;122:1–10. https://doi.org/10.1016/j.fgb.2018.10.001
[24] Katoh K, Rozewicki J, Yamada K. MAFFT online service: multiple sequence alignment, interactive sequence choice and visualization. Brief Bioinform 2017;20(4):1160–6. https://doi.org/10.1093/bib/bbx108
[25] Kumar S, Stecher G, Tamura K. MEGA7: molecular evolutionary genetics analysis version 7.0 for bigger datasets. Mol Biol Evol 2016;33(7):1870–4. https://doi.org/10.1093/molbev/msw054
[26] Alves R, Sousa-Silva M, Vieira D, Soares P, Chebaro Y, Lorenz M, et al. Carboxylic acid transporters in *Candida* pathogenesis. MBio 2020;11(3):e00156-20. https://doi.org/10.1128/mBio.00156-20
[27] Gietz R, Woods R. Yeast transformation by the LiAc/SS Carrier DNA/PEG method. Yeast Protocols. Springer; 2006. p. 107–20. https://doi.org/10.1385/1-59259-958-3:107
[28] Jacobus AP, Gross J. Optimal cloning of PCR fragments by homologous recombination in *Escherichia coli*. PLoS One 2015;10(3):e0119221. https://doi.org/10.1371/journal.pone.0119221
[29] Zimmermann L, Stephens A, Nam S, Rau D, Kübler J, Lozajic M, et al. A completely reimplemented MPI bioinformatics toolkit with a new HHpred server at its core. J Mol Biol 2018;430(15):2237–43. https://doi.org/10.1016/j.jmb.2017.12.007
[30] Varadi M, Anyango S, Deshpande M, Nair S, Natassia C, Yordanova G, et al. AlphaFold Protein Structure Database: massively expanding the structural coverage of protein-sequence space with high-accuracy models. Nucleic Acids Res 2022;50(D1):D439–44. https://doi.org/10.1093/nar/gkab1061
[31] Bosshart P, Kalbermatter D, Bonetti S, Fotiadis D. Mechanistic basis of L-lactate transport in the SLC16 solute carrier family. Nat Commun 2019;10(1):1–11. https://doi.org/10.1038/s41467-019-10566-6
[32] Pettersen E, Goddard T, Huang C, Couch G, Greenblatt D, Meng E, et al. UCSF Chimera—a visualization system for exploratory research and analysis. J Comput Chem 2004;25(13):1605–12. https://doi.org/10.1002/jcc.20084
[33] Dallakyan S, Olson A. Small-molecule library screening by docking with PyRx. Chemical biology. Springer; 2015. p. 243–50. https://doi.org/10.1007/978-1-4939-2269-7_1
[34] Rendulić T, Alves J, Azevedo-Silva J, Soares-Silva I, Casal M. New insights into the acetate uptake transporter (AceTr) family: unveiling amino acid residues critical for specificity and activity. Comput Struct Biotechnol J 2021;19:4412–25. https://doi.org/10.1016/j.csbj.2021.08.002
[35] Smart O, Neduvelil J, Wang X, Wallace B, Sansom M. HOLE: a program for the analysis of the pore dimensions of ion channel structural models. J Mol Graph 1996;14(6):354–60. https://doi.org/10.1016/S0263-7855(97)00009-X
[36] Humphrey W, Dalke A, Schulten K. VMD: visual molecular dynamics. J Mol Graph 1996;14(1):33–8. https://doi.org/10.1016/0263-7855(96)00018-5
[37] Erian AM, Egermeier M, Marx H, Sauer M. Insights into the glycerol transport of *Yarrowia lipolytica*. Yeast 2022;39(5):323–36. https://doi.org/10.1002/yea.3702
[38] Partow S, Siewers V, Bjorn S, Nielsen J, Maury J. Characterization of different promoters for designing a new expression vector in *Saccharomyces cerevisiae*. Yeast 2010;27(11):955–64. https://doi.org/10.1002/yea.1806
[39] Nunes P, Tenreiro S, Sá-Correia I. Resistance and adaptation to quinidine in *Saccharomyces cerevisiae*: role of QDR1 (YIL120w), encoding a plasma membrane transporter of the major facilitator superfamily required for multidrug resistance. Antimicrob Agents Chemother 2001;45(5):1528–34. https://doi.org/10.1128/AAC.45.5.1528-1534.2001
[40] Vargas R, Tenreiro S, Teixeira M, Fernandes A, Sá-Correia I. *Saccharomyces cerevisiae* multidrug transporter Qdr2p (Yil121wp): localization and function as a quinidine resistance determinant. Antimicrob Agents Chemother 2004;48(7):2531–7. https://doi.org/10.1128/AAC.48.7.2531-2537.2004
[41] Tenreiro S, Nunes P, Viegas C, Neves M, Teixeira M, Cabral M, et al. *AQR1* gene (ORF YNL065w) encodes a plasma membrane transporter of the major facilitator superfamily that confers resistance to short-chain monocarboxylic acids and quinidine in *Saccharomyces cerevisiae*. Biochem Biophys Res Commun 2002;292(3):741–8. https://doi.org/10.1006/bbrc.2002.6703
[42] Velasco I, Tenreiro S, Calderon I, André B. *Saccharomyces cerevisiae* Aqr1 is an internal-membrane transporter involved in excretion of amino acids. Eukaryot Cell 2004;3(6):1492–503. https://doi.org/10.1128/EC.3.6.1492-1503.2004
[43] Tenreiro S, Vargas R, Teixeira M, Magnani C, Sá-Correia I. The yeast multidrug transporter Qdr3 (Ybr043c): localization and role as a determinant of resistance to quinidine, barban, cisplatin, and bleomycin. Biochem Biophys Res Commun 2005;327(3):952–9. https://doi.org/10.1016/j.bbrc.2004.12.097
[44] Felder T, Bogengruber E, Tenreiro S, Ellinger A, Sá-Correia I, Briza P. Dtr1p, a multidrug resistance transporter of the major facilitator superfamily, plays an essential role in spore wall maturation in *Saccharomyces cerevisiae*. Eukaryot Cell 2002;1(5):799–810. https://doi.org/10.1128/EC.1.5.799-810.2002
[45] Casal M, Paiva S, Queirós O, Soares-Silva I. Transport of carboxylic acids in yeasts. FEMS Microbiol Rev 2008;32(6):974–94. https://doi.org/10.1111/j.1574-6976.2008.00128.x
[46] Peña A, Sánchez N, Álvarez H, Calahorra M, Ramírez J. Effects of high medium pH on growth, metabolism and transport in *Saccharomyces cerevisiae*. FEMS Yeast Res 2015;15(2). https://doi.org/10.1093/femsyr/fou005
[47] Halestrap A. Monocarboxylic acid transport. Compr Physiol 2011;3(4):1611–43. https://doi.org/10.1002/cphy.c130008
[48] Cássio F, Leão C. Low-and high-affinity transport systems for citric acid in the yeast *Candida utilis*. Appl Environ Microbiol 1991;57(12):3623–8. https://doi.org/10.1128/aem.57.12.3623-3628.1991
[49] Cássio F, Leão C. A comparative study on the transport of L (-) malic acid and other short-chain carboxylic acids in the yeast *Candida utilis*: Evidence for a general organic acid permease. Yeast 1993;9(7):743–52. https://doi.org/10.1002/yea.320090708
[50] Roberts SK, Milnes J, Caddick M. Characterisation of AnBEST1, a functional anion channel in the plasma membrane of the filamentous fungus, *Aspergillus nidulans*. Fungal Genet Biol 2011;48(9):928–38. https://doi.org/10.1016/j.fgb.2011.05.004
[51] Xi Y, Zhan T, Xu H, Chen J, Bi C, Fan F, et al. Characterization of JEN family carboxylate transporters from the acid-tolerant yeast *Pichia kudriavzevii* and their applications in succinic acid production. Microb Biotechnol 2021;14(3):1130–47. https://doi.org/10.1111/1751-7915.13781
[52] Sousa-Silva M, Soares P, Alves J, Vieira D, Casal M, Soares-Silva I. Uncovering novel plasma membrane carboxylate transporters in the yeast *Cyberlindnera jadinii*. J Fungi 2022;8(1):51. https://doi.org/10.3390/jof8010051
[53] Vargas R, García-Salcedo R, Tenreiro S, Teixeira M, Fernandes A, Ramos J, et al. *Saccharomyces cerevisiae* multidrug resistance transporter Qdr2 is implicated in potassium uptake, providing a physiological advantage to quinidine-stressed cells. Eukaryot Cell 2007;6(2):134–42. https://doi.org/10.1128/EC.00290-06
[54] Dos Santos S, Teixeira M, Dias P, Sá-Correia I. MFS transporters required for multidrug/multixenobiotic (MD/MX) resistance in the model yeast: understanding their physiological function through post-genomic approaches. Front Physiol 2014;5:180. https://doi.org/10.3389/fphys.2014.00180
[55] Zhang X, Nijland JG, Driessen AJM. Combined roles of exporters in acetic acid tolerance in *Saccharomyces cerevisiae*. Biotechnol Biofuels Bioprod 2022;15(1):67. https://doi.org/10.1186/s13068-022-02164-4
[56] Andersen M, Salazar M, Schaap P, van de Vondervoort P, Culley D, Thykaer J, et al. Comparative genomics of citric-acid-producing *Aspergillus niger* ATCC 1015 versus enzyme-producing CBS 513.88. Genome Res 2011;21(6):885–97. https://doi.org/10.1101/gr.112169.110
[57] Pel H, De Winde J, Archer D, Dyer P, Hofmann G, Schaap P, et al. Genome sequencing and analysis of the versatile cell factory *Aspergillus niger* CBS 513.88. Nat Biotechnol 2007;25(2):221–31. https://doi.org/10.1038/nbt1282
[58] Halestrap A. The SLC16 gene family–structure, role and regulation in health and disease. Mol Asp Med 2013;34(2–3):337–49. https://doi.org/10.1016/j.mam.2012.05.003